# Solving lattice density functionals close to the Mott regime

Zu-Jian Ying,[1,2,*] Valentina Brosco,[1,3] and José Lorenzana[1]

[1]*Istituto dei Sistemi Complessi, CNR and Università di Roma "La Sapienza," P. le A. Moro 2, I-00185 Rome, Italy*

[2]*Beijing Computational Science Research Center, Beijing 100084, China*

[3]*SPIN-CNR and Universitá di Roma "La Sapienza," P. le A. Moro 2, I-00185 Rome, Italy*

(Received 22 March 2014; revised manuscript received 6 May 2014; published 27 May 2014)

We study a lattice version of the local density approximation (LDA) based on Bethe ansatz (BALDA). Contrary to what happens in density functional theory in the continuum and despite its name, BALDA displays some very nonlocal features and it has a discontinuous functional derivative. The same features prevent the convergence of the self-consistent Kohn-Sham cycle thus hindering the study of BALDA solutions close to a Mott phase or in the Coulomb blockade regime. Here, we propose a numerical approach which, differently from previous works, does not introduce *ad hoc* parameters to smear out the singularity. Our results are relevant for all lattice models where BALDA is applied ranging from Kondo systems to harmonically trapped Hubbard fermions. As an example, we apply the method to the study of a one-dimensional lattice model with Hubbard interaction and a staggered potential which can be driven from an ionic to a Mott-insulating state. In the Mott regime, the presence of a "vacuum" allows us to calculate the different contribution to the gap and to highlight an ultranonlocality of BALDA.

DOI: 10.1103/PhysRevB.89.205130 PACS number(s): 71.10.Fd, 71.15.Mb, 71.27.+a

## I. INTRODUCTION

The extension of density functional theory (DFT) to treat lattice fermions dates back to the 1980s and it has been recently the subject of a revived interest [1–33]. One motivation to develop lattice DFT (LDFT) is that it provides a "sandbox" environment where one can study the subtleties of DFT itself, clarify the origin of inaccuracies in approximate functionals [1–13], and test ideas on new functionals [11]. Another motivation is provided by the problem of solving lattice models in the presence of an inhomogeneous potential. Lattice models are at the basis of our understanding of the phenomenology of strongly correlated, magnetic, and disordered systems. Their fundamental relevance has in recent years motivated a number of successful experiments with ultracold atomic gases in optical lattices [34–36] fueling at the same time the development and refinement of efficient theoretical tools (see, e.g., [37]) among which LDFT has become particularly useful [21,38,39]. Static and time-dependent [14–16] lattice DFT were indeed used to investigate the physics of Hubbard models with onsite interaction [13,17–22], Kondo models [23–28], disordered interacting lattice models [31,32], and spin liquids [33].

The local density approximation (LDA) is the commonest approximation to the exchange-correlation (xc) functional of DFT, already proposed by Hohenberg and Kohn [40], it was first applied to a lattice model by Gunnarsson and Schönhammer [3,7] and subsequently by Lima *et al.* [10]. In the case of the one-dimensional Hubbard model, there is the advantage that the exact solution of the homogeneous reference model is known by Bethe ansatz [41] (BA). One can thus base the LDA on the exact energy or use the approximate but accurate analytical expressions available [7,9,10,17]. One intriguing aspect of such Bethe ansatz LDA (BALDA) functional is that, differently from the standard continuum LDA, it has a discontinuous functional derivative. Such nonanalytic behavior stems directly from electron correlation and it has important consequences on the relation between the charge gap and the gap in the Kohn-Sham (KS) spectrum [13,42–50]. Furthermore, as it will be explained in the following, it is ultimately responsible for an ultranonlocality of BALDA, which is absent in standard continuum LDA.

Derivative discontinuities and the associated cusp singularities in the exchange-correlation energy undermine the convergence of self-consistent KS equations. So far, various approaches have been proposed to solve this problem for the BALDA functional including smoothening of the cusp minimum by going to a finite temperature [19] or by adding an *ad hoc* parameter [20,24] or by relying on Thomas-Fermi approximation [22]. Here, we present a solution which allows us to treat in a simple and clean manner the cusp singularity of the BALDA functional at zero temperature: instead of the site occupation, we use the LDA local chemical potential as a variable and we develop self-consistent equations.

As an example, we apply our method, which we call $\mu$-BALDA, to a Hubbard model subject to a staggered spin-independent site potential, also known as the ionic Hubbard model [10,51–53] (IHM). At half-filling, by modifying the ratio between Hubbard interaction and the staggered potential, it can be tuned continuously from an ionic to a Mott-insulating regime [51,54]. In both regimes, we calculate the xc potential and the charge gap by applying $\mu$-BALDA.

The paper is organized as follows. In Sec. II, we give a description of the model and of the basics of lattice DFT. In Sec. III, we present a brief review of BALDA, we explain how the cusp problem emerges, and we introduce the $\mu$-BALDA algorithm. We then apply our method to the IHM in Sec. IV. As a proxy to a solid with a surface we study a bulk system with high binding energy attached to a zero binding energy chain representing the vacuum [13]. This geometry allows us to have a well-defined KS potential at all sites, even those with integer density, and to highlight an ultranonlocal behavior of LDA in the lattice, computing also the different contributions to the charge gap in the discontinuous situation. We conclude in Sec. V.

*Corresponding author: zujianying@gmail.com

 

## II. LATTICE DENSITY FUNCTIONAL THEORY

Let us start by outlining of the basics of LDFT. We consider a Hubbard chain in an inhomogeneous static field $v_x$:

$$H = -t\sum_{x\sigma}(c^\dagger_{x\sigma}c_{x+1\sigma} - n_{x\sigma} + \text{H.c.}) + U\sum_x n_{x\uparrow}n_{x\downarrow} + \sum_{x\sigma} v_x n_{x\sigma}, \quad (1)$$

where $c^\dagger_{x\sigma}$ creates an electron with spin $\sigma = \uparrow,\downarrow$ at site $x$ and $n_{x\sigma} = c^\dagger_{x\sigma}c_{x\sigma}$, while $U$ and $t$ are, respectively, the interaction constant and the hopping amplitude. Notice that we have included an onsite contribution in the definition of the "kinetic energy," i.e., in the first term on the right-hand side of Eq. (1). With this choice and "external potential" $v_x = 0$, the lowest-energy one-particle state has zero energy in analogy with the continuum model. This will be useful below to simulate a "vacuum" region (Sec. IV).

As in standard Kohn-Sham continuum DFT [55], also in lattice DFT, the total ground-state energy can be obtained by minimizing a functional written as the sum of three density-dependent terms

$$E = T_{\text{KS}} + E_{\text{Hxc}} + E_v, \quad (2)$$

where $T_{\text{KS}}$ is Kohn-Sham kinetic energy functional, $E_{\text{Hxc}}$ is the Hartree-exchange-correlation (Hxc) functional, and

$$E_v = \sum_x v_x\rho_x,$$

with $\rho_x \equiv \langle n_x\rangle$ denoting the density at site $x$. Notice that the "functional" is actually a multivariable function of the onsite densities $\rho_x$. The functional $E_{\text{Hxc}}$ is "universal" in that it does not depend on the external potential $v_x$.

Minimization of the functional with the constraint $\sum_x \rho_x = N$ leads to the KS equations

$$[\hat{t} + v^s_x]\varphi_{\kappa,x} = \varepsilon^N_\kappa\varphi_{\kappa,x}, \quad (3)$$

where $\hat{t}$ denotes the hopping operator $\hat{t}\varphi_{\kappa,x} = -t(\varphi_{\kappa,x-1} + \varphi_{\kappa,x+1} - 2\varphi_{\kappa,x})$ and $\varepsilon^N_\kappa$ indicates the $\kappa$th eigenvalue of the $N$-particle system and $\kappa = k\sigma$ includes the orbital $k$ and spin components. The KS potential is defined as

$$v^s_x = v^{\text{Hxc}}_x + v_x. \quad (4)$$

Even if not explicitly indicated, $v^s_x$ and $v^{\text{Hxc}}_x$ depend on the number of particles $N$. In the lattice formulation, the functional derivative with respect to the density becomes a partial derivative with respect to the onsite density [2,29] leading to the following definition of the Hxc potential:

$$v^{\text{Hxc}}_x = \frac{\partial E_{\text{Hxc}}}{\partial\rho_x}. \quad (5)$$

The ground-state density of $N$ particles is composed of all occupied KS orbitals

$$\rho_x = \sum_{\kappa\in\text{occ.}} \varphi^*_{\kappa,x}\varphi_{\kappa,x}. \quad (6)$$

Since the $v^{\text{Hxc}}_x$ is a functional of the total density, Eqs. (3) and (6) have to be solved self-consistently.

Due to the constraint on the total number of particles, the Hxc potential is defined up to a constant both in the continuum and in the lattice. One can extend DFT by considering ensemble densities [42,49,50,56]. In this case, even the constant term in $v^{\text{Hxc}}_x$ is determined.

Intrinsic to the ensemble formulation of DFT are derivative discontinuities of the exchange-correlation energy functional which arise when the total density crosses an integer $N$. As first discussed by Perdew *et al.* [42], these lead to a discontinuous uniform change $\Delta_{\text{xc}}$ in the KS potential $v^s_x$ when an integer filling is approached from the left or from the right, namely,

$$\Delta_{\text{xc}} = v^{\text{Hxc}}_x(N^+) - v^{\text{Hxc}}_x(N^-), \quad (7)$$

where $N^\pm = N\pm\eta$ with $\eta = 0^+$. It can be shown that the charge gap of the system $\Delta_c \equiv E_0(N+1) + E_0(N-1) - 2E_0(N)$, with $E_0(N)$ the $N$-particle ground-state energy, satisfies

$$\Delta_c = \Delta_{\text{KS}} + \Delta_{\text{xc}}, \quad (8)$$

where $\Delta_{\text{KS}} = \varepsilon^N_{N+1} - \varepsilon^N_N$ is the single-particle Kohn-Sham gap. Another important result is the DFT version of Koopman's theorem which is valid both in the continuum [43,57] and in the lattice [13] and it relates the highest occupied Kohn-Sham eigenvalue $\varepsilon^N_N$ to the ionization energy

$$I_N = -\varepsilon^N_N, \quad (9)$$

where $I_N \equiv E_0(N-1) - E_0(N)$. One can also show [58] that if particles are bound in a finite region of space around the origin, $v^{\text{Hxc}}_x \to 0$ when $x\to\infty$, such that $\rho_x \to 0$.

## III. BETHE ANSATZ LOCAL DENSITY APPROXIMATION

Within BALDA, the Hxc energy functional is approximated by a sum of local contributions as follows [9,10,59]:

$$E_{\text{Hxc}} = \sum_x e^{\text{Hxc}}_x = \sum_x [e^{\text{hom}}(U,\rho_x) - e^{\text{hom}}(0,\rho_x)], \quad (10)$$

where $e^{\text{hom}}(U,\rho)$ is the energy *per* site of the standard Hubbard model defined as

$$H_H = -t\sum_{x\sigma}(c^+_{x\sigma}c_{x+1\sigma} + \text{H.c.}) + U\sum_x n_{x\uparrow}n_{x\downarrow}. \quad (11)$$

We do not include here the onsite term in the kinetic energy which does not affect Eq. (10) but it affects the zero of the homogeneous chemical potential defined in the following.

In the one-dimensional case, the energy of the uniform system can be calculated exactly for all fillings by BA [41] and one can easily relate the appearance of a finite $\Delta_{\text{xc}}$ to the presence of a cusp singularity in the BA energy density $e^{\text{hom}}(U,\rho)$ at $\rho = 1$. The physical consequences of this nonanalytic behavior and the solutions of the related technical difficulties in the implementation of KS-DFT are the subject of the following sections. Most of the results presented below can be generalized to higher dimension using numerical solutions of the uniform many-body problem.

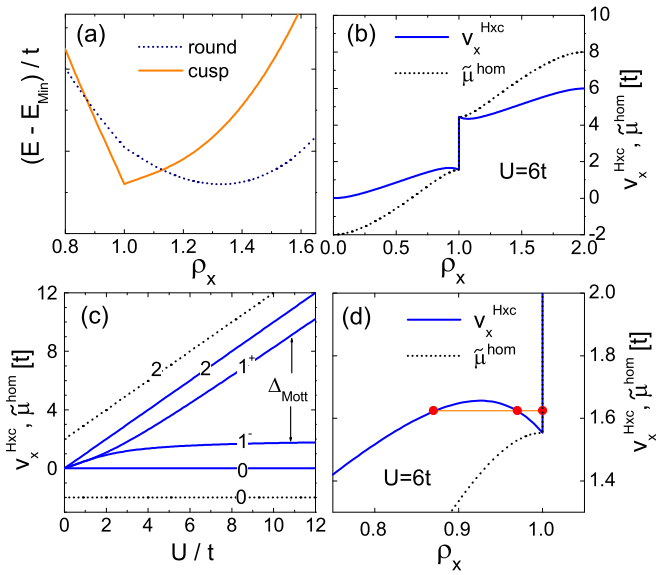


FIG. 1. (Color online) (a) Examples of cusp and round minima in BALDA for $U = 6t$ (cusp), $U = 3t$ (round) in the presence of an ionic potential of amplitude $V = 1t$. In the presence of an inhomogeneous potential, both situations coexist on the same system. (b) Hxc and chemical potentials $v_x^{\rm Hxc}$ and $\tilde{\mu}_x$, as functions of the site occupation for $U = 6t$ and $v_x = 0$. (c) $v_x^{\rm Hxc}$ (full line) and $\tilde{\mu}_x$ (dotted line) as functions of the interaction strength. Curves are labeled by the onsite occupation $\rho_x$. In the case of $\rho_x = 1^{\pm}$, the two quantities coincide (only $v_x^{\rm Hxc}$ shown). (d) A zoom of panel (b) around $\rho_x = 1$ to compare the nonmonotonous behavior of $v_x^{\rm Hxc}$ with the monotonous behavior of $\tilde{\mu}_x$.

### A. Cusp problem and $\mu$-Bethe-ansatz local density approximation

Most difficulties in the implementation of BALDA are related to the fact that BA energy $e^{\rm hom}(U,\rho)$ has a cusp at $\rho = 1$. The implications for BALDA functional are evident in Fig. 1(a) where we show two energy curves describing the typical dependence of BALDA energy on the occupation $\rho_x$ of a site: when the energy minimum with respect to $\rho_x$ is located away or at $\rho_x = 1$, the functional has, respectively, a round or a cusp behavior at equilibrium. In the latter case, the Hxc potential is a discontinuous functional of the density and, as recently discussed in Ref. [19], the convergence of KS self-consistent cycle is not guaranteed. More precisely, when the density of a site is away from half-filling, $\rho_x \neq 1$, the Hxc potential is obtained as usual as the derivative of the Hxc energy [Eqs. (5), (10)]

$$v_x^{\rm Hxc} = \tilde{\mu}^{\rm hom}(U,\rho_x) - \tilde{\mu}^{\rm hom}(0,\rho_x), \tag{12}$$

where the local chemical potential $\tilde{\mu}^{\rm hom}(U,\rho)$ coincides with the chemical potential of a homogeneous system with density $\rho$ and interaction $U$:

$$\tilde{\mu}^{\rm hom}(U,\rho_x) = \frac{\partial e^{\rm hom}}{\partial \rho_x}(U,\rho_x). \tag{13}$$

On the contrary, for $\rho_x = 1$, the standard definition given in Eq. (12) becomes ambiguous, indeed the derivative of $e^{\rm hom}(U,\rho)$ has a jump whose amplitude equals the Mott gap $\Delta_{\rm Mott}^{\rm hom}$ of the uniform system. This leads to numerical instabilities if one uses a standard approach to solve Kohn-Sham equations.

Notice that Eqs. (12) and (13) together with the definition of Eq. (11) imply that $v^{\rm Hxc}$ and $\tilde{\mu}^{\rm hom}$ have the same limits when $\rho \to 1^{\pm}$, as shown in Fig. 1(b). We can thus define $v_{\rm Hxc}^{\pm} = \tilde{\mu}_{\pm}^{\rm hom}$ and we have $\tilde{\mu}_{+}^{\rm hom} - \tilde{\mu}_{-}^{\rm hom} = v_{\rm Hxc}^{+} - v_{\rm Hxc}^{-} = \Delta_{\rm Mott}^{\rm hom}$. Figure 1(c) shows $v_{\rm Hxc}^{+}$, $v_{\rm Hxc}^{-}$ (full lines labeled $1^{\pm}$) as a function of $U/t$.

Notice also that not only one value of the density ($\rho_x = 1$) corresponds to a continuum of values of $v_{\rm Hxc}$, but also certain values of $v_{\rm Hxc}$ correspond to three values of the density as one can see in Fig. 1(d), which may lead to additional numerical problems.

As mentioned in the Introduction, various methods have been developed to treat these problems: some modify the BALDA functional relying on a sort of Thomas-Fermi approximation [20,24], others entail the introduction of an *ad hoc* parameter [22] or a finite temperature to smoothen the discontinuity [19].

Here, we propose a different route which allows us to solve the KS equations self-consistently without any additional parameter. Instead of $\rho_x$, we take the chemical potential of the homogeneous system as a variable, in this sense we name our method by $\mu$-BALDA. Since, as shown in Fig. 2(a), the chemical potential in Eq. (13) is a monotonous function of the density Eq. (13) can be inverted. Using $\tilde{\mu}_x$ as the independent variable (to avoid confusion with the function $\tilde{\mu}^{\rm hom}$), the inverse can then be written as

$$\rho_x = \rho_x^{\rm hom}(U,\tilde{\mu}_x). \tag{14}$$

The inverse function $\rho_x^{\rm hom}(U,\tilde{\mu}_x)$, shown schematically in Fig. 2(b), does not have discontinuities but it has plateaus for $\mu_x$ inside the Mott gap and above the upper and below the lower Hubbard band, i.e., for $\rho_x = 0,1,2$. Inserting Eq. (14) in (12), we obtain the LDA Hxc potential in terms of $\tilde{\mu}_x$:

$$v_x^{\rm Hxc}(\tilde{\mu}_x) = \tilde{\mu}_x - \tilde{\mu}^{\rm hom}\big[0,\rho_x^{\rm hom}(U,\tilde{\mu}_x)\big]. \tag{15}$$

This function is shown schematically by the blue dashed line in Fig. 2(b). The advantage of this change of variable becomes clear when we compare Eq. (12) with (15). In the former, the potential is a discontinuous function of the independent variable $\rho$, while in the latter it is a continuous function of the variable $\mu_x$ as shown in the two panels of Fig. 2. Indeed, the last term in Eq. (15) is the chemical potential of the noninteracting system, which has no discontinuity and it simply becomes constant when $\rho$ is constant, i.e., in the plateau regions. The plateaus then simply map into a linear behavior of $v_x^{\rm Hxc}(\tilde{\mu}_x)$ which is continuous and well defined for all values of $\tilde{\mu}_x$ as shown by the dashed line in Fig. 2(b). As we will discuss in the following, curing the discontinuity solves the convergence problem.

According to the Hohenberg and Kohn theorem [1,40], and its lattice generalization [2,59], the interacting ground-state density determines uniquely (up to a constant) the noninteracting potential that yields the same density as the interacting one, which should hold regardless of the presence or absence of cusps (except [2,59] in the trivial case of total filling $\rho = 2$). The KS equations (3) together with prescription given in Eq. (6) yield the noninteracting density

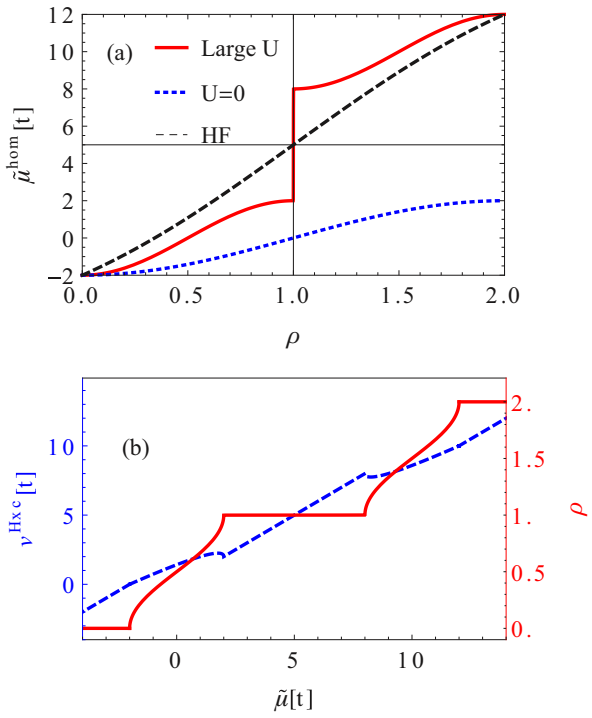


FIG. 2. (Color online) (a) Uniform chemical potential for large $U$ as a function of filling. According to Ogata and Shiba [60] in the $U/t \to \infty$ the system can be mapped to a spinless fermion model. Therefore, the chemical potential for $0 < \rho < 1$ has a simple sine behavior. At $\rho = 1$, the chemical potential jumps by the Mott gap. In the picture we took $U = 10$ to have a finite gap. For $\rho > 1$, the chemical potential has again a sine form. For comparison, we also plot the chemical potential of noninteracting electrons and the HF chemical potential. (b) The red full line (right scale) is the density as a function of the chemical potential inverting the corresponding curve in panel (a). The dashed line (left scale) illustrates the behavior of the exchange-correlation potential as a function of local chemical potential [Eq. (15)].

as a functional of the Hxc potential $\rho_x = \rho_x[v^{\rm Hxc}]$, where the square brackets abbreviate the multivariable functions, i.e., we set $\rho_x(v_1^{\rm Hxc}, \ldots, v_L^{\rm Hxc}) = \rho_x[v^{\rm Hxc}]$.

Inserting Eq. (15) in (3), we obtain the density as functional of the local chemical potential $\tilde{\mu}_x$, i.e.,

$$\rho_x = \rho_x[v^{\rm Hxc}(\tilde{\mu})]. \tag{16}$$

Finally, to obtain self-consistency, we request that this density coincides with the density from Eq. (14):

$$F_x[\tilde{\mu}] \equiv \rho_x[v^{\rm Hxc}(\tilde{\mu})] - \rho_x^{\rm hom}(U, \tilde{\mu}_x) = 0. \tag{17}$$

Before proceeding, we stress that, as indicated by the square and round brackets on the right-hand side of Eq. (16), in spite of the local approximation used to define the potential $v^{\rm Hxc}$, the relation between $\rho$ and $\tilde{\mu}$ is nonlocal. Generally, one can expect that the density from Eq. (16) decreases if the local $v^{\rm Hxc}$ increases. This follows simply from the fact that this variation is governed by the noninteracting compressibility which must be positive. Since $v^{\rm Hxc}$ is an almost monotonous increasing function of the local chemical potential $\tilde{\mu}_x$, the local density in Eq. (16) should decrease when $\tilde{\mu}_x$ increases. Instead, the density as a function of $\tilde{\mu}_x$ from Eq. (14) is manifestly an increasing function of $\tilde{\mu}_x$. This warrants that the curves defined by Eqs. (14) and (16) should cross at some value of $\tilde{\mu}_x$ when one $\tilde{\mu}_x$ is changed. The only potential problem may occur for $\tilde{\mu}_x$ just below and above the Mott gap region, where there is a small region of nonmonotonous behavior of Eq. (15) [dashed line in Fig. 2(b)]. In principle, this may lead to multiple solutions, but in all numerical implementations we never found this problem.

While the above arguments do not warrant the convergence when all $\tilde{\mu}_x$ are moved simultaneously, it is clear that the main problem related to the discontinuity in Eq. (12) is not there any more.

In practice, Eqs. (17) can be solved iteratively starting from some initial guess for the chemical potentials $\mu_x^{(0)}$. Here, we expand $F_x$ to arrive at a set of linear recursive equations:

$$F_x[\tilde{\mu}^{(r-1)}] + \nabla_{\tilde{\mu}} F_x[\tilde{\mu}]|_{\tilde{\boldsymbol{\mu}}=\tilde{\boldsymbol{\mu}}^{(r-1)}} \cdot (\tilde{\boldsymbol{\mu}}^{(r)} - \tilde{\boldsymbol{\mu}}^{(r-1)}) = 0, \tag{18}$$

where we defined the vector $\tilde{\boldsymbol{\mu}} = (\tilde{\mu}_1, \ldots \tilde{\mu}_L)$. The gradient in Eq. (18) can be computed analytically using perturbation theory or numerically from finite differences. We found the latter option to be faster. For a reasonable initial set $\tilde{\mu}_x^{(0)}$, Eqs. (18) converge rapidly to the final solution while, in the presence of cusps, the conventional KS iteration scheme does not converge.

We stress that our algorithm treats the cusp and normal sites in a unified way. One does not need to assume or guess beforehand which site will be a cusp. If the self-consistent solution $\tilde{\mu}_x$ falls inside (outside) the range $[\tilde{\mu}_-^{\rm hom}, \tilde{\mu}_+^{\rm hom}]$, the site $x$ is a cusp (normal) site [see Fig. 4(a)]. This range corresponds to the central plateau in the full curve of Fig. 2(b). Being in the plateau region ensures that such sites have $\rho_x = 1$. The Kohn-Sham potential is determined implicitly by Eq. (16) with the density of the cusp sites on the left fixed to $\rho_x = 1$. The Kohn-Sham potential for noncusp sites, instead, is determined by the usual stationary condition which leads to Eq. (5). Thus, in all sites the Kohn-Sham potential is well defined.

To understand the results discussed below concerning the inhomogeneous potential case, it is useful to discuss the behavior of $\tilde{\mu}^{\rm hom}$ and $v^{\rm Hxc}$ in the uniform case as a function of interaction strength and filling. At zero filling [curves labeled 0 in Fig. 1(c)] and independently of interaction strength, it is easy to see that our definitions lead to $v^{\rm Hxc} = 0$ (solid blue curve) and $\tilde{\mu}^{\rm hom} = -2t$ (dashed line). For larger fillings at a given interaction strength, $v^{\rm Hxc}$ increases due to the effective repulsion among particles.

For small $U$, the Hxc potential is dominated by the Hartree part and it behaves as $v^{\rm Hxc} \approx U\rho_x/2$. This behavior is clear up to $U/t \sim 2$ from the curves labeled $1^{\pm}$ in Fig. 1(c) which represent $v_{\rm Hxc}^{\pm}$. For larger $U/t$, the two curves clearly diverge. Such difference is actually present for any $U/t$ (but exponentially small for small $U/t$) and represents the Mott gap. Furthermore, for large interaction, $v_{\rm Hxc}^{-}$ tends to a constant while $v_{\rm Hxc}^{+}$ increases linearly with $U$. The limiting value of $v_{\rm Hxc}^{-}$ can be understood from the fact that the charge sector of the uniform Hubbard model can be mapped [60] for large $U$ to a spinless fermion model with bandwidth $4t$ describing the lower Hubbard band for $\rho_x < 1$. This point is also clear from Fig. 2(a) where we see that, as the filling increases, the "large-$U$" chemical potential changes from $-2t$ for zero

filling to $2t$ for filling $\rho = 1^-$ while the HF chemical potential increases linearly. Notice that the behavior of the exact BA chemical potential $\tilde{\mu}^{\rm hom}$ for $U = 6t$ shown in Fig. 1(b) is well approximated by the "large-$U$" chemical potential. We also see that $v_{\rm Hxc}$ has the same limiting values as $\tilde{\mu}^{\rm hom}$ for $\rho \to 1^{\pm}$. For $\rho_x = 1^+$, both the chemical potential and $v_{\rm Hxc}$ jump by an amount equal to the Hubbard gap which is of order $\Delta_{\rm Mott} = U - 4t$ in this limit. The behavior for filling larger than 1 can be understood using particle-hole symmetry.

The fact that $v^{\rm Hxc}(\rho_x < 1)$ saturates for large $U$ (instead of having the naive mean-field behavior $v^{\rm Hxc} = U\rho_x/2$) is typical of approaches where correlations are taken into account so electrons can avoid the large Coulomb cost. The present picture can be compared with similar results obtained using Gutzwiller approximation [see Fig. 1(c) of Ref. [61]). There, the self-energy and the uniform chemical potential for filling $\rho_x < 1$ saturate at large $U$ and they jump by the Mott gap on passing from $\rho_x = 1^-$ to $1^+$. One can interpret the limiting value of $v^{\rm Hxc}(\rho_x < 1)$ as the effect of a residual kinematic interaction between quasiparticles in the lower Hubbard band.

## IV. APPLICATION TO THE IONIC HUBBARD MODEL

We now apply $\mu$-BALDA to the study of the ionic Hubbard model (IHM), a Hubbard model with onsite interaction and a staggered potential. In closed lattice models, the single-particle potential that yields the ground-state density of the interacting system is determined up to a constant since adding a constant to the potential leaves the charges invariant. In open systems which have a "vacuum" region one can fix the constant in such a way that the potential vanishes when both the density and the external potential vanish, far from the region where the particles are bound. In Ref. [13], we considered the open system shown in Fig. 3, with a vacuum region to completely determine the exact Hxc potential of the "bulk" Hubbard chain from a knowledge of the exact density.

In BALDA, in principle, the zero of the Hxc potential is determined by the explicit expression (12). However, as explained above, the potential is not determined by this expression when $\rho_x = 1$, thus to remove any ambiguity on the potential we find it useful to consider the same geometry as in Ref. [13]. It will become clear in the following that in reality the vacuum region is not essential but it is enough to have just one site in the system in which $\rho_x \neq 1$ to completely determine the potential. Still, we use the geometry of Ref. [13] which is conceptually simple and analogous to the real situation in a solid. In addition, this geometry (or any geometry with a confining potential) presents a challenge to conventional algorithms because, as we shall see, cusp sites coexist with noncusp sites.

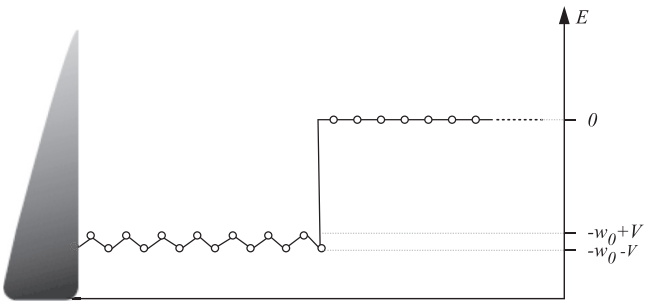


FIG. 3. Schematic picture of the model studied.

Specifically, we consider a Hubbard chain of $L_B$ sites with a large binding energy, called "the bulk," followed by a chain of $L_V$ sites with zero binding energy, termed "the vacuum," with open boundary conditions. The external potential $v_x$ includes both a steplike potential which accounts for the "work function" of the "solid" and the staggered field

$$v_x = -[w_0 + V(-1)^x]\theta(L_B - x + 1/2),$$

where $w_0 > 0$ denotes the well depth and $V > 0$ is the amplitude of the staggered field. Here, we study the model around half-filling and we consider both the band-insulating (BI) and the Mott-insulating phase (MI), the latter appearing when the Hubbard interaction $U$ dominates over the staggered potential $U \gtrsim 2V$ (see, e.g., Refs. [13,51,54]).

### A. Shift in the exchange-correlation potential and ultranonlocality of the lattice local density approximation

Figure 4 shows the Hxc potential [panels (a) and (b)] and the density [panels (c) and (d)] when the bulk chain is half-filled ($N = L_B$) and when one particle is added or subtracted with respect to half-filling ($N = L_B \pm 1$).

At half-filling and for large onsite repulsion, the bulk is in the Mott phase and the system becomes nearly incompressible. It therefore does not react to the staggered potential and all bulk sites have charge $\rho_x \sim 1$ [orange line in Figs. 4(c) and 4(d)]. When this occurs, the KS potential becomes nearly constant in the bulk and $v^{\rm Hxc}$ acquires a staggered component behaving as $V(-1)^x$ which "screens" out the external potential, as shown in Figs. 4(a) and 4(b). This is a strong correlation effect captured by BALDA, as opposed to LDA in the continuum which would

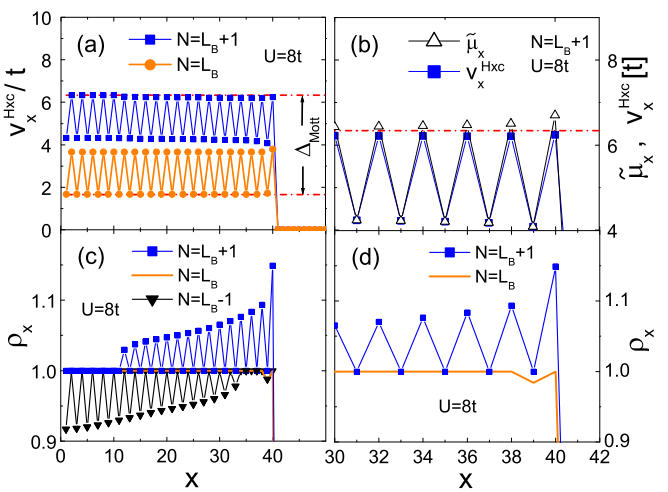


FIG. 4. (Color online) Panels (a) and (c): behavior of the local Hxc potential $v_x^{\rm Hxc}$ and of the density $\rho_x$ for $N = L_B$ and $L_B \pm 1$ with $U = 8t$, $w_0 = 10t$, $V = t$, $L_B = 40$, and $L_V = 20$. Panels (b) and (d) are a zoom of panels (a) and (c) where we only plot for $N = L_B$ and $L_B + 1$ and we also show the local chemical potential $\tilde{\mu}_x$. The dashed-dotted lines in panels (a) and (b) indicate the potentials $\tilde{\mu}_+^{\rm hom}$ and $\tilde{\mu}_-^{\rm hom}$.

not be able to describe a similar situation in a heteroatomic chain of atoms.

What determines the value of $v^{\mathrm{Hxc}}$ in the bulk with respect to the vacuum? On a closer look at the density in Fig. 4(d) one sees that a small amount of charge leaks to the vacuum from the site with $x = 39$, which is the site with small ionization energy closer to the surface. Having a density smaller than 1, this site is not affected by the cusp problem and it has a well-defined Hxc potential $v_{39}^{\mathrm{Hxc}} \approx v_{\mathrm{Hxc}}^{-} \approx 2t$. Moreover, since the density has to be homogeneous and all the sites must have nearly the same effective potential, the Hxc potential of the other odd sites will be also very close to $v_{\mathrm{Hxc}}^{-}$ while the Hxc potential of the even sites has to satisfy the relation $v_{2x}^{\mathrm{Hxc}} = v_{\mathrm{Hxc}}^{-} + 2V$, so that $v_{2x}^{s} \simeq v_{2x+1}^{s} \simeq v_{\mathrm{Hxc}}^{-} + V$. Notice that all these sites are cusp sites with $\rho_x = 1$, so their Hxc potential is not determined by the *local* relation (12) but by the ultranonlocal condition that all sites need to have the same density. In other words, due to Eq. (16), the condition that the densities of certain sites is fixed to 1 corresponds to a highly nonlocal condition for the potential and it is fulfilled through a readjustment of the potential on all other sites as dictated by Eqs. (17). Our numerical algorithm correctly converges to this solution with a mixture of cusp and noncusp sites.

For $N = L_B + 1$, the role of odd and even sites is reversed. Indeed, as shown by the squares in Fig. 4(c) in this case, some of the even sites have a density slightly above 1 and, having their Hxc potential determined by Eq. (12), they play the role of reference sites while the odd sites have all unitary occupations and their potential is fixed by the even sites potential. In this case, we have $v_{2x}^{\mathrm{Hxc}} = v_{\mathrm{Hxc}}^{+}$ and $v_{2x+1}^{\mathrm{Hxc}} = v_{\mathrm{Hxc}}^{+} - 2V$. The case $N = L_B - 1$ is very similar to the case $N = L_B$, in this case, as explained above, some of the odd sites have a density slightly below 1 and they play the role of reference sites.

From the above discussion, we conclude that the external staggered potential is screened in the even sites for $N = L_B, L_B - 1$ and in the odd sites when $N = L_B + 1$. The net result is that $v_{\mathrm{Hxc}}$ jumps by a constant quantity of order of $\Delta_{\mathrm{xc}} \sim \Delta_{\mathrm{Mott}}^{\mathrm{hom}} - 2V$, with $\Delta_{\mathrm{Mott}}^{\mathrm{hom}} \sim U - 4t$ and where we used the fact that $v_{\mathrm{Hxc}}^{+} - v_{\mathrm{Hxc}}^{-} = \Delta_{\mathrm{Mott}}^{\mathrm{hom}}$. The relation with the charge gap will be discussed in Sec. IV B.

It is easy to compute the exact ionization energies in the atomic limit directly from Eq. (1) setting $t = 0$. In order to satisfy Koopmans theorem and in the case of a bulk uniform system (as found in the Mott regime), the exact KS potential in the bulk should satisfy $v_x^s = -I$. Therefore, in this limit we can obtain the exact xc potential quite easily. Interestingly, the KS potentials obtained by $\mu$-BALDA converge to the same results as shown next.

At half-filling ionization occurs from odd sites leading to $I \simeq w_0 - V$ and $v^s \sim -w_0 + V$ in agreement with the $\mu$-BALDA results. In the case $N = L_B + 1$ (shown with blue lines in Fig. 4), the added charge will reside mainly on the even sites ($v_x = -w_0 - V$) so that ionization will occur from these sites. In the atomic limit in the Mott regime one obtains $I = w_0 + V - U$. This leads to $v^s \sim -w_0 - V + U$ which implies $v_{2x+1}^{\mathrm{Hxc}} \sim U - 2V \sim v_{\mathrm{Hxc}}^{+} - 2V$ and $v_{2x}^{\mathrm{Hxc}} \sim v_{\mathrm{Hxc}}^{+}$, again in agreement with the $\mu$-BALDA results.

Let us conclude the discussion of Fig. 4 with a technical remark. In the exact many-body solution, only the uniform compressibility is zero but the compressibility is small but finite at finite momentum. Therefore, differently from what is predicted by BALDA, in the exact solution, for all $V \neq 0$ the charge imbalance between odd and even sites is nonvanishing. For large $U/t$, however, the deviations from the BALDA $\rho_x = 1$ solution are expected to be small, the compressibility being trivially zero at all momenta in the atomic limit.

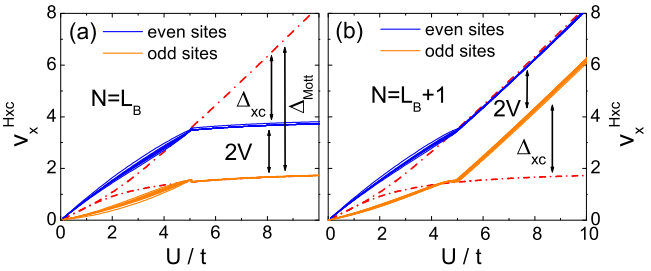


FIG. 5. (Color online) Hxc potential of even (upper blue band) and odd sites (lower orange band) across the Mott transition for fillings of $N = L_B$ (a) and $N = L_B + 1$ (b) for $L_B = 20$, $L_V = 20$, and $w_0 = 15t$. The dashed-dotted lines represent $v_{\mathrm{Hxc}}^{+}$ and $v_{\mathrm{Hxc}}^{-}$ whose difference equals the Mott gap $\Delta_{\mathrm{Mott}}$.

Figure 5 shows how the xc potential of odd and even sites evolves from the band-insulating regime at small interaction to the Mott-insulating regime at large interaction. In the band-insulator regime, the xc potential tends to screen the external potential but it lies outside the interval $[v_{\mathrm{Hxc}}^{-}, v_{\mathrm{Hxc}}^{+}]$ marked by the dotted-dashed red lines. In this regime, the occupation of the sites is larger or smaller than 1. As the interaction increases, the system becomes less compressible and the charges tend to approach one. When the xc potential of the different sites (blue and orange curves) hits the dotted-dashed red lines (or more precisely the $\mu_x$ fall inside $[\tilde{\mu}_{+}^{\mathrm{hom}}, \tilde{\mu}_{-}^{\mathrm{hom}}]$), the system enters the Mott-insulating regime. The density becomes homogeneous and the difference between the odd and even site potentials equals $2V$. Depending on whether the reference sites have a density smaller or larger than 1, even sites align to $v_{\mathrm{Hxc}}^{-}$ (a) or odd sites align to $v_{\mathrm{Hxc}}^{+}$ (b).

We stress again that the above results show how, within BALDA, strong correlation leads to an *ultranonlocality* of the Hxc potential. The potential of the whole system is indeed fixed by the presence of just one or few sites whose density is slightly below or above half-filling. As mentioned above, it is enough to have a single site in the system with density different from 1 to obtain the absolute value of the xc potential in all sites. Leakage to the vacuum is a natural way to obtain such a reference site, but an impurity would work as well. For a large periodic closed system, the absolute value of the xc potential can be determined by a limiting procedure considering small deviations from half-filling from below or from above.

### B. Charge gap

As stated in Eq. (8), the fundamental charge gap $\Delta_c$ can be written as the sum of two terms, the KS gap $\Delta_s$, and a contribution coming from the discontinuity of $v_{\mathrm{xc}}$ upon the addition of an infinitesimal amount of charge to the system [Eq. (7)]. The latter is site independent and it can be calculated, in some simple cases even analytically [13,62]. A rigorous definition of the discontinuity in $v_{\mathrm{xc}}$ requires using ensemble DFT [49,50,56]. Alternatively, $\Delta_{\mathrm{xc}}$ can be estimated

employing a formula first derived by Sham and Schlüter in Ref. [44], based on finite differences, which reads as

$$\Delta_{\rm xc} \simeq \Delta_{\rm xc}^{N,N+1} = \sum_x \left[v_x^{\rm xc}(N+1) - v_x^{\rm xc}(N)\right]\rho_{N+1,x}^N, \quad (19)$$

where $\rho_{N+1}^N$ is the $(N+1)$th KS orbital density for $N$ particles and $v_x^{\rm xc}(N)$ denotes the xc potential of the $N$-particle system at site $x$. The difference between $v^{\rm xc}(N)$ and $v^{\rm xc}(N+1)$ on the right-hand side of the above equation is in general site dependent due to the fact that the charge added is finite.

The estimate of Eq. (19), which we adopt here, converges to the exact result of Eq. (7) when the local change in the density upon addition of an electron becomes infinitesimally small, as in extended systems in the thermodynamic limit. Eventually, we remark that a simple expression of the error $\Delta_{\rm xc}^{N,N+1} - \Delta_{\rm xc}$ can be obtained along the lines of the Supplemental Material of Ref. [13].

We now come to the discussion of $\mu$-BALDA results for the charge gap. As mentioned in the Introduction, the ionic Hubbard model displays a transition between an ionic and a Mott-insulating regime. As thoroughly discussed in a number of papers (see, e.g., Ref. [54] and references therein), the Mott regime appears when the Hubbard interaction dominates over the staggered potential and the charge gap has a minimum at the transition point.

In Fig. 6, we plot the charge gap (obtained as total energy differences) as a function of $V$ [Fig. 6(a)] and $U$ [Fig. 6(b)] obtained with $\mu$-BALDA and compared to practically exact numerical results. In the Mott regime, the charge gap equals the xc discontinuity and the $\mu$-BALDA KS gap $\Delta_{\rm KS}$ vanishes as the density becomes homogeneous. On the contrary, in the ionic regime the charge gap approximately coincides with the KS gap while the xc discontinuity becomes vanishingly small, since in this regime there are no half-filled sites.

Taking into account that the $\mu$-BALDA solution is homogeneous in the Mott phase, we can give an analytical expression for the behavior of the $\mu$-BALDA charge gap in the Mott regime. In this case, the charge gap in Eq. (8) is exhausted by the discontinuity in the potential obtained in the previous section,

$$\Delta_c = \Delta_{\rm Mott}^{\rm hom} - 2V \simeq U - 4t - 2V, \quad (20)$$

where the last expression is valid for large $U/t$. In the large-$U$ limit, the critical value of the potential is given by

$$V_c = (U - 4t)/2. \quad (21)$$

Clearly, the transition from the Mott regime to the band-insulating regime occurs when $V \approx 3.0t$ in $\mu$-BALDA and $V \approx 4.3t$ in Lanczos [Fig. 6(a)].

Equations (20) and (21) explain the linear behavior observed in the explicit solution of $\mu$-BALDA in the Mott regime [small $V$ in Fig. 6(a) and large $U$ in Fig. 6(b)] and also the critical values $V_c \approx 3t$ in Fig. 6(a) and $U_c = 2V + 4t \approx 6t$. The latter result overestimates the exact critical $U$ on Fig. 6(b) which we attribute to the inaccuracy of the large-$U$ approximation at the critical value.

In general, BALDA underestimates the charge gap in the Mott regime [small $V$ in Fig. 6(a) and large $U$ in Fig. 6(b)] and it fails to describe the nonlinear dependence of the gap for small $V$ [Fig. 6(a)]. These failures can be related to the fact

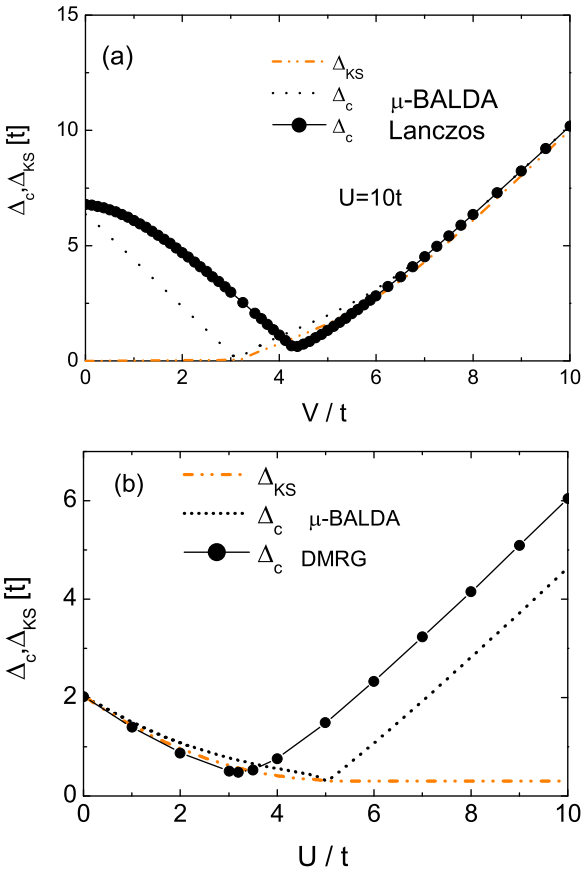


FIG. 6. (Color online) (a) Charge gap $\Delta_c$ as a function of $V$ for a half-filled ring of $L = 12$ sites with $U = 10t$ and periodic boundary conditions. We also show exact results obtained with Lanczos exact diagonalization [63]. (b) Charge gap $\Delta_c$ (dashed blue line) and KS gap $\Delta_{KS}$ (dotted-dashed orange line) calculated with $\mu$-BALDA. The results are obtained for $L_B = 20$, $L_V = 20$, and $w_0 = 15t$ and $V = t$. For comparison, also the DMRG [63] charge gap is shown (dotted black line).

that in the Mott regime, BALDA tends to generate a ground state which is more homogeneous than the true one as we remarked in the previous section. The inhomogeneity in the exact density will be associated to a small Kohn-Sham gap in the exact Kohn-Sham spectrum which will tend to diminish the discrepancy. For large $V$ in the band-insulating regime, the $\mu$-BALDA charge gap rapidly converges to the exact result which approximately coincides with the KS gap. This shows that in the band-insulating regime, despite the strong interaction, BALDA works remarkably well.

It is interesting to notice that Eqs. (20) and (21) converge to the exact result in the atomic limit $t = 0$. In this case, the charge gap is given by $\Delta_c \simeq |U - 2V|$ and the transition occurs at $U \simeq 2V$.

## V. CONCLUSIONS AND DISCUSSIONS

Probably one of the most popular LDFT approaches called BALDA has until now required *ad hoc* regularizations of the xc energy to describe the Mott phase. In this work, we have solved

this long-standing problem, developing a method to find the exchange-correlation potential of a lattice system in the Mott regime with a fully self-consistent procedure. Differently from previous works, our algorithm, which we call $\mu$-BALDA, uses the local chemical potentials as variables. As an example, we apply the method to the study of the transition between Mott- and band-insulating regimes of the ionic Hubbard model. Aside from the general methodological progress, we obtain several results: (i) we have shown that in the Mott regime the external potential is completely screened by the xc potential; (ii) we highlight an ultranonlocality of LDA in the lattice, i.e., we show that in the presence of the discontinuity, one or few "reference sites" in the system are capable of fixing the whole xc potential; (iii) we calculate separately the different contribution to the gap in the different regimes providing, in particular, an analytical understanding of the behavior of the $\mu$-BALDA charge gap in the Mott regime; (iv) in the Mott phase, due to correlation, ionization occurs from different sites for a system slightly below or above half-filling. This gives a contribution to the ionization energy which can not be captured in a single-particle picture but which is captured by $\mu$-BALDA. Aside from these nice qualitative features, we have discussed the quantitative errors of BALDA in the Mott regime and the high accuracy in the band-insulating regime even when the interaction is not small.

In this paper, we extract the energy of the homogeneous system from exact BA [41], but the method can be clearly also applied when the approximate analytical parametrization introduced by Lima *et al.* [9,10] is used. Our results are therefore relevant for all one-dimensional lattice models where BALDA is applied, including Kondo systems [23,25–28], dynamical Coulomb blockade treated with time-dependent DFT [24], harmonically trapped Hubbard electrons [19,22,33], and spinless fermions with neighboring interaction [18]. $\mu$-BALDA is actually a rather general approach and it could be in principle generalized also to higher dimensions or to treat other discontinuous functionals.

## ACKNOWLEDGMENTS

This work was supported by the Italian Institute of Technology through the project NEWDFESCM. V.B. acknowledges financial support by MIUR under Grant No. FIRB2012 (RBFR1236VV).

[1] W. Kohn, Phys. Rev. Lett. **51**, 1596 (1983).
[2] J. T. Chayes, L. Chayes, and M. Ruskai, J. Stat. Phys. **38**, 497 (1985).
[3] O. Gunnarsson and K. Schönhammer, Phys. Rev. Lett. **56**, 1968 (1986).
[4] R. López-Sandoval and G. M. Pastor, Phys. Rev. B **67**, 035115 (2003).
[5] R. López-Sandoval and G. M. Pastor, Phys. Rev. B **69**, 085101 (2004).
[6] M. Saubanère and G. M. Pastor, Phys. Rev. B **79**, 235101 (2009).
[7] K. Schönhammer, O. Gunnarsson, and R. M. Noack, Phys. Rev. B **52**, 2504 (1995).
[8] A. Schindlmayr and R. W. Godby, Phys. Rev. B **51**, 10427 (1995).
[9] N. A. Lima, L. N. Oliveira, and K. Capelle, Europhys. Lett. **60**, 601 (2002).
[10] N. A. Lima, M. F. Silva, L. N. Oliveira, and K. Capelle, Phys. Rev. Lett. **90**, 146402 (2003).
[11] J. Lorenzana, Z.-J. Ying, and V. Brosco, Phys. Rev. B **86**, 075131 (2012).
[12] E. M. Stoudenmire, Lucas O. Wagner, Steven R. White, and Kieron Burke, Phys. Rev. Lett. **109**, 056402 (2012).
[13] V. Brosco, Z.-J. Ying, and J. Lorenzana, Sci. Rep. **3**, 2172 (2013).
[14] I. V. Tokatly, Phys. Rev. B **83**, 035127 (2011).
[15] M. Farzanehpour and I. V. Tokatly, Phys. Rev. B **86**, 125130 (2012).
[16] A. Akande and S. Sanvito, J. Phys.: Condens. Matter **24**, 055602 (2012).
[17] V. V. França, D. Vieira, and K. Capelle, New J. Phys. **14**, 073021 (2012).
[18] S. Schenk, M. Dzierzawa, P. Schwab, and U. Eckern, Phys. Rev. B **78**, 165102 (2008).
[19] X. Gao, A.-Hai Chen, I. V. Tokatly, and S. Kurth, Phys. Rev. B **86**, 235139 (2012).
[20] D. Karlsson, A. Privitera, and C. Verdozzi, Phys. Rev. Lett. **106**, 116401 (2011).
[21] V. L. Campo, K. Capelle, J. Quintanilla, and C. Hooley, Phys. Rev. Lett. **99**, 240403 (2007).
[22] G. Xianlong, M. Polini, M. P. Tosi, V. L. Campo, K. Capelle, and M. Rigol, Phys. Rev. B **73**, 165120 (2006).
[23] C. Verdozzi, Phys. Rev. Lett. **101**, 166401 (2008).
[24] S. Kurth, G. Stefanucci, E. Khosravi, C. Verdozzi, and E. K. U. Gross, Phys. Rev. Lett. **104**, 236801 (2010).
[25] G. Stefanucci and S. Kurth, Phys. Rev. Lett. **107**, 216401 (2011).
[26] F. Evers and P. Schmitteckert, Phys. Chem. Chem. Phys. **13**, 14417 (2011).
[27] P. Tröster, P. Schmitteckert, and F. Evers, Phys. Rev. B **85**, 115409 (2012).
[28] J. P. Bergfield, Z. F. Liu, K. Burke, and C. A. Stafford, Phys. Rev. Lett. **108**, 066801 (2012).
[29] K. Capelle and V. L. Campo, Phys. Rep. **528**, 91 (2013).
[30] F. Heidrich-Meisner, G. Orso, and A. E. Feiguin, Phys. Rev. A **81**, 053602 (2010).
[31] V. Vettchinkina, A. Kartsev, D. Karlsson, and C. Verdozzi, Phys. Rev. B **87**, 115117 (2013).
[32] A. Kartsev, D. Karlsson, A. Privitera, and C. Verdozzi, Sci. Rep. **3**, 02570 (2013).
[33] G. Xianlong, M. Rizzi, M. Polini, R. Fazio, M. P. Tosi, V. L. Campo, and K. Capelle, Phys. Rev. Lett. **98**, 030404 (2007).
[34] I. Bloch, J. Dalibard, and W. Zwerger, Rev. Mod. Phys. **80**, 885 (2008).
[35] T. Esslinger, Annu. Rev. Condens. Matter Phys. **1**, 129 (2010).
[36] I. Bloch, J. Dalibard, and S. Nascimbene, Nat. Phys. **8**, 267 (2012).
[37] M. Lewenstein *et al.*, Adv. Phys. **56**, 243 (2007).
[38] V. W. Scarola, L. Pollet, J. Oitmaa, and M. Troyer, Phys. Rev. Lett. **102**, 135302 (2009).

[39] S. Fuchs, E. Gull, L. Pollet, E. Burovski, E. Kozik, T. Pruschke, and M. Troyer, Phys. Rev. Lett. **106**, 030401 (2011).
[40] P. Hohenberg and W. Kohn, Phys. Rev. **136**, B864 (1964).
[41] E. H. Lieb and F. Y. Wu, Phys. Rev. Lett. **20**, 1445 (1968).
[42] J. P. Perdew, R. G. Parr, M. Levy, and J. L. Balduz, Phys. Rev. Lett. **49**, 1691 (1982).
[43] J. P. Perdew and M. Levy, Phys. Rev. Lett. **51**, 1884 (1983).
[44] L. J. Sham and M. Schlüter, Phys. Rev. Lett. **51**, 1888 (1983).
[45] L. J. Sham and M. Schlüter, Phys. Rev. B **32**, 3883 (1985).
[46] R. W. Godby, M. Schlüter, and L. J. Sham, Phys. Rev. Lett. **56**, 2415 (1986).
[47] L. J. Sham and M. Schlüter, Phys. Rev. Lett. **60**, 1582 (1988).
[48] M. Grüning, A. Marini, and A. Rubio, J. Chem. Phys. **124**, 154108 (2006).
[49] A. J. Cohen, P. Mori-Sánchez, and W. Yang, Science **321**, 792 (2008).
[50] W. Yang, A. J. Cohen, and P. M. Sánchez, J. Chem. Phys. **136**, 204111 (2012).
[51] N. Nagaosa and T. Jun-ichi, J. Phys. Soc. Jpn. **55**, 2735 (1986).
[52] J. Zaanen, G. A. Sawatzky, and J. W. Allen, Phys. Rev. Lett. **55**, 418 (1985).
[53] C. A. Balseiro, M. Avignon, A. G. Rojo, and B. Alascio, Phys. Rev. Lett. **62**, 2624 (1989).
[54] S. R. Manmana, V. Meden, R. M. Noack, and K. Schönhammer, Phys. Rev. B **70**, 155115 (2004).
[55] W. Kohn and L. J. Sham, Phys. Rev. **140**, A1133 (1965).
[56] P. Mori-Sánchez, A. J. Cohen, and W. Yang, Phys. Rev. Lett. **100**, 146401 (2008).
[57] C. O. Almbladh and A. C. Pedroza, Phys. Rev. A **29**, 2322 (1984).
[58] M. Levy, J. P. Perdew, and V. Sahni, Phys. Rev. A **30**, 2745 (1984).
[59] W. Kohn, Rev. Mod. Phys. **71**, 1253 (1999).
[60] M. Ogata and H. Shiba, Phys. Rev. B **41**, 2326 (1990).
[61] G. Seibold, F. Becca, and J. Lorenzana, Phys. Rev. Lett. **100**, 016405 (2008).
[62] P. Gori-Giorgi and A. Savin, Int. J. Quantum Chem. **109**, 2410 (2009).
[63] B. Bauer *et al.*, J. Stat. Mech. (2011) P05001.